Van Damme A., Degryse F., Smolders E., Sarret G., Dewit J., Swennen R. & Manceau A. (2010) Zinc speciation in mining and smelter contaminated overbank sediments by EXAFS spectroscopy. *Geochimica et Cosmochimica Acta* 74: 3707-3720.

Author manuscript

The definitive version is available through www.sciencedirect.com

doi:10.1016/j.gca.2010.03.032

ZINC SPECIATION IN MINING AND SMELTER CONTAMINATED OVERBANK SEDIMENTS BY EXAFS SPECTROSCOPY

An Van Damme[a,*], Fien Degryse[b], Erik Smolders[b], Géraldine Sarret[c], Julie Dewit[a], Rudy Swennen[a], Alain Manceau[d]

[a] *Geology Section, Department of Earth and Environmental Sciences, K.U.Leuven, Celestijnenlaan 200E, 3001 Heverlee, Belgium*

[b] *Division Soil and Water Management, Department of Earth and Environmental Sciences, K.U.Leuven, Kasteelpark Arenberg 20, 3001 Heverlee, Belgium*

[c] *Environmental Geochemistry Group, LGIT, University Joseph Fourier and CNRS, 38041 Grenoble Cedex 9, France*

[d] *Mineralogy & Environments, LGCA, University Joseph Fourier and CNRS, 38041 Grenoble Cedex 9, France*

* *Corresponding author: An.VanDamme@ees.kuleuven.be*

Abstract

Overbank sediments contaminated with metalliferous minerals are a source of toxic metals that pose risks to living organisms. The overbank sediments from the Geul river in Belgium contain 4000 to 69000 mg/kg Zn as a result of mining and smelting activities, principally during the 19th century. Three main Zn species were identified by powder Zn K-edge EXAFS spectroscopy: smithsonite ($ZnCO_3$), tetrahedrally coordinated sorbed Zn (sorbed ^{IV}Zn), and Zn-containing trioctahedral phyllosilicate. Smithsonite is a primary mineral, which accounts for approximately 20 to 60 % of the Zn in sediments affected by mining and smelting of oxidized Zn ores (mostly carbonates and silicates). This species is almost absent in sediments affected by mining and smelting of both sulphidic (ZnS, PbS) and oxidized ores, presumably because of acidic dissolution associated with the oxidation of sulphides, as suggested by the lower pH of this second type of sediment ($pH(CaCl_2) < 7.0$ vs. $pH(CaCl_2) > 7.0$ for the first type). Thus, sulphide minerals in sediment deposits can act as a secondary source of dissolved metals by a chemical process analogous to acid-mine drainage. The sorbed ^{IV}Zn component ranges up to approximately 30 %, with the highest proportion occurring at $pH(CaCl_2) < 7.0$ as a result of the readsorption of dissolved Zn^{2+} on sediments constituents. Kerolite-like Zn-rich phyllosilicate is the major secondary species in all samples, and in some the only detected species, thus providing the first evidence for pervasive sequestration of Zn into this newly formed precipitate at the field scale.

1. INTRODUCTION

Historical mining and smelting of metal ores often heavily affected the local environment in the neighbourhood of extraction and production sites. In the area of the Geul river (E-Belgium and S-Netherlands), approximately 1.1 million tons of zinc and 0.13 million tons of lead were produced during the 19th century and the beginning of the 20th century (Dejonghe et al., 1993, 1998), resulting in elevated concentrations of Zn, Pb and Cd in the nearby overbank and river sediments (Leenaers, 1989; Swennen et al., 1994; Stam, 2002). Because overbank sediments are deposited nearly horizontally on floodplain surfaces, analysis of sediment layers provides a historical record of the river contamination (Ottesen et al., 1989; Miller and Orbock Miller, 2007).

Zinc contamination may present risks for living organisms. Since the bioavailability, mobility and toxicity of metal contaminants strongly depend on their chemical forms, a detailed knowledge of their speciation is required to evaluate their impact on ecosystems. The weathering of primary Zn-minerals releases aqueous Zn^{2+}, which can be sorbed on soil constituents, such as organic matter, Fe- and Mn-(oxyhydr)oxides and clay minerals, or precipitated with other solute species, such as Si to form a Zn-rich phyllosilicate, Al to form a layered double hydroxide (Zn-LDH), or even carbonates to form hydrozincite. The nature of these primary and secondary Zn-containing phases has been studied extensively by powder Zn K-edge EXAFS (extended X-ray absorption fine structure) spectroscopy (Manceau et al., 2002; D'Amore et al., 2005) in soils and sediments contaminated by mining and smelting operations, weathering of galvanization products, and application on land of dredged sediments and sewage sludges (Manceau et al., 2000; Isaure et al., 2002, 2005; Roberts et al., 2002; Scheinost et al., 2002; Sarret et al., 2004; Panfili et al., 2005; Nachtegaal et al., 2005; Kirpichtchikova et al., 2006; Schuwirth et al., 2007; Jacquat et al., 2008, 2009). These studies provided insight into how the nature of the secondary Zn species is influenced by the local chemical conditions, including soil pH, Zn concentration relative to the type and amount of sorption sites, Si and Al concentrations, and CO_2 partial pressure.

This work further documents the distribution of Zn between primary minerals, sorbed species and newly formed precipitates at the field scale. Two representative vertical profiles in the overbank sediments of the Geul river were studied to obtain information on the temporal evolution (<200 years) of mineral weathering and transformation reactions. Historical relationships between sediment deposition, contamination source and speciation are discussed to advance understanding of the geochemistry of Zn in this environmental system.

2. MATERIALS AND METHODS

2.1. Site description and sampling

Overbank and river sediment samples were collected from the catchment of the Geul river. The two most important mines along the Geul river were Plombières (named Bleiberg in German) and La Calamine (named Kelmis in German) (Fig. 1). Pre-industrial mining already occurred during the Middle Ages. Mining and smelting activities reached their apogee in the middle of the 19th century, and ceased in 1884. The smelters were located nearby the mines. Smelting of imported ores and mining at other locations continued in the first decades of the 20th century. Even today, metals are still introduced into the river system through the weathering and erosion of waste dumps (Kucha et al., 1996) and remobilization of contaminated overbank sediments. The ore minerals are composed predominantly of galena (PbS) and sphalerite (ZnS) at Plombières and several other smaller mines, and of a mixture of oxidized minerals, including smithsonite ($ZnCO_3$), hemimorphite ($Zn_4Si_2O_7(OH)_2.H_2O$) and willemite (Zn_2SiO_4) at La Calamine.

The samples were taken in the Belgian part of the catchment (Fig. 1), where the Geul river is incised in Palaeozoic sandstone, dolomite, limestone and shale (Swennen and Viaene, 1990). Vertical profiles were sampled on two locations in the overbank sediments. The cut banks, more than 2 m high, were sampled over 1–20 cm depth intervals within discrete sedimentary units. The first profile (LC samples) is situated ~1 km downstream of the former mine of La Calamine and upstream of Plombières, and thus received dominantly oxidized Zn minerals from La Calamine. The second sampling site (PB samples) is located downstream of the two mines, ~7 km from La Calamine and ~2

km from Plombières, and received both oxidized and Pb-Zn sulphide minerals from the mines in the area. In addition, a sample of river sediment (i.e. today's bedload) was collected near the border between Belgium and the Netherlands, ~4 km downstream of the ancient mining centre of Plombières.

2.2. Analytical methods

All samples were dried at 30°C and passed through a 2 mm sieve. Total element concentrations were determined by atomic absorption spectroscopy (AAS) for Zn, Pb, Mn, Fe, Ca, Mg, K and Al, and by inductively coupled plasma mass spectrometry (ICP-MS) for Cd, As and Cu, after hot acid digestion ($HCl/HNO_3/HF$). Total S was measured with a Ströhlein Sulfur Analyser. Organic carbon was analysed by the Walkley and Black method (Nelson and Sommers, 1982). The pH, referred to as pH(water), was measured in a sediment/water suspension of 1/2.5 kg/L. Grain size was determined by laser diffraction after physical (disaggregation) and chemical (decalcification, removal of Fe and organic matter) pretreatment (Horckmans et al., 2007). Mineralogical analyses were performed by X-ray diffraction (XRD, using CuKα radiation) on bulk samples and/or concentrates, separated by sieving (125–250 µm), density ($d > 2.9$ g/mL) and magnetic fractionation (Van Herreweghe et al., 2002).

Single extractions with 0.01 M $CaCl_2$ (sediment to solution ratio of 1/10 kg/L) were performed following the procedure of the EC Standards, Measurements and Testing Programme (Quevauviller, 1998). Zinc concentrations and pH, referred to as pH($CaCl_2$), were measured in the solutions. The pH($CaCl_2$) was lower than the pH(water) by 0.6 unit on average. The $CaCl_2$ extract mimics the soil solution with respect to pH and ionic strength, and is therefore often used to predict the solid–liquid distribution of metals in soils (Houba et al., 1996; Degryse et al., 2003). The aqueous Zn concentrations in equilibrium with smithsonite ($ZnCO_3$) and with Zn-kerolite ($Si_4Zn_3O_{10}(OH)_2.nH_2O$) in a 0.01 M $CaCl_2$ solution were calculated using MINTEQA2 v. 4.0 (Allison et al., 1991) for a CO_2 partial pressure of 10^{-3} atm and a Si concentration of 10^{-4} M. Since the accuracy of the solubility product of Zn-kerolite is relatively low ($\log K = 8 \pm 6$; Manceau et al., 2000; Panfili et al., 2005), the saturation concentration of Zn in equilibrium with Zn-kerolite was calculated for $\log K = 8$ and 12.

2.3. Powder Zn K-edge EXAFS spectroscopy

Powder Zn K-edge X-ray absorption spectra were measured at room temperature on beamline BM26A (DUBBLE ; Nikitenko et al., 2008) at the European Synchrotron Radiation Facility (ESRF, Grenoble, France). The beam energy was calibrated with a Zn foil before the start of the measurements. Data were collected from pressed pellets in transmission mode using ionization chambers for concentrated samples ([Zn] > 10000 mg/kg) and in fluorescence mode using a 9-element Ge-detector for diluted samples ([Zn] < 10000 mg/kg). The pellets were oriented at 45° from the incident X-ray beam, thus at an angle close enough to the 35° "magic angle" to cancel any possible effects from preferential orientation (Manceau et al., 1990). Multiple scans were averaged to increase signal-to-noise ratios. Spectra were acquired on 0–2 mm bulk fractions, on 1–2 mm and 125–250 µm size fractions separated from the 0–2 mm fraction by dry sieving, and on the 0–2 µm size fraction separated from the 0–2 mm fraction by centrifugation.

EXAFS spectra were extracted from X-ray absorption spectra by normalizing the signal amplitude to the jump in absorbance at the K-edge and by simulating the post-edge total absorption with a spline function. The kinetic energy (E_k) of the photoelectron was converted to wave vector (k) values by taking the energy origin ($E_k = 0$) at the half-height of the absorption jump. Data were reduced using the software code Athena (Newville, 2001; Ravel and Newville, 2005). The number of components (i.e. Zn species) necessary to reproduce the complete set of k^3-weighted EXAFS spectra was determined by principal component analysis (PCA; Wasserman et al., 1999; Ressler et al., 2000; Manceau et al., 2002). The number of meaningful components was evaluated with five criteria: the indicator parameter IND, the total normalized sum-square residual (NSS_{tot}) defined as the sum of the squares of the residuals normalized to the sum of the squares of the data values over all points in the dataset, the marginal decrease of NSS_{tot} upon addition of a new component, and visual inspections of the components and spectral reconstructions (Malinowski, 1977, 1978; Manceau and Matynia, 2010). Then, Zn species were identified by target transformation, a procedure to evaluate whether a reference spectrum is a likely component of the dataset. Two criteria were used for this assessment: the NSS of the reconstruction to the original reference spectrum, and the visual comparison of the two

spectra. Finally, the fractional amounts of the total Zn among all forms in the samples were determined by linear combination fitting (LCF) of the experimental EXAFS spectra with the reference spectra positively identified by target transformation. An additional species was added to the LCF reconstruction if the NSS decreased by at least 10 %. PCA and LCF were performed using the approach and softwares developed by A. Manceau and M.A. Marcus on beamline 10.3.2 of the Advanced Light Source (ALS, Berkeley, US; Manceau et al., 1996, 2002; Marcus et al., 2004). All spectra were analysed over the 2.5–10.5 $Å^{-1}$ *k*-interval.

A database of Zn minerals, Zn-substituted and Zn-sorbed references, and Zn organic compounds was used to identify Zn species. The database contained smithsonite (from a natural sample), willemite, hemimorphite, franklinite, gahnite (Scheinost et al., 2002), sphalerite (Schuwirth et al., 2007), zincite (Voegelin et al., 2005), hydrozincite (Jacquat et al., 2008), a series of Zn-containing kerolites ($Si_4(Zn_xMg_{3-x})O_{10}(OH)_2.nH_2O$) with x = 0.03, 1.35 or 3.00 (Manceau et al., 2000; Schlegel et al., 2001a) or x = 2.40 (Voegelin et al., 2005), trioctahedral Zn-phyllosilicate precipitated at the layer edges of montmorillonite, Zn-sorbed montmorillonite (Schlegel and Manceau, 2006), natural Zn-substituted Redhill montmorillonite (Manceau et al., 2005), Zn layered double hydroxide (Zn-LDH, $Zn_2Al(OH)_6Cl$; Voegelin et al., 2005), Zn-substituted goethite (Manceau et al., 2000), Zn-sorbed ferrihydrite, Zn-reacted gibbsite (Roberts et al., 2002), Zn-reacted hydroxylapatite at pH 5 and pH 6 and at various metal concentrations (Panfili et al., 2005), Zn parahopeite, Zn acetate, Zn citrate, Zn malate, Zn oxalate, Zn phytate, Zn sorbed on humic and fulvic acids at various concentrations, and aqueous Zn ($ZnNO_3$ solution at pH 4) (Sarret et al., 2002, 2004).

3. RESULTS

3.1. Chemical and mineralogical composition

Characteristics of the samples are reported in Table 1. The samples have a pH(water) between 6.7 and 8.0 and an organic carbon content between 0.4 and 4.4 %. The Zn concentration ranges from 3200 mg/kg to 69000 mg/kg. Contamination undoubtedly results from the past mining and smelting activities because the overbank sediments at 5 km upstream of La Calamine contain less than 400 mg/kg (data not shown). The LC profile is the most contaminated in zinc, with Zn concentrations above 10000 mg/kg. The Zn pattern shows two maxima, 69000 mg/kg at 168–183 cm depth (LC04) and 47000 mg/kg at 93–108 cm depth (LC09) (not shown). The highest concentrations of Pb (5400 mg/kg), Cd (29 mg/kg), As (89 mg/kg) and Cu (73 mg/kg) are reached in the upper part of the PB profile (<59 cm), consistent with the mining and smelting of Pb-Zn sulphides in Plombières (Swennen et al., 1994). The bulk sediments contain mainly quartz, as determined by XRD, and also some dolomite and aluminosilicates (microcline, albite). Zinc-minerals identified by XRD in the overbank sediments and the present-day river sediment are smithsonite, hemimorphite and willemite (Table 1). Sphalerite was detected only in the river sediment. No Pb-bearing phase was detected by XRD.

3.2. Identification of Zn species

The whole set of powder Zn K-edge EXAFS spectra is shown in Fig. 2. The spectra were classified in two groups based on their shape, and thus nature of the main Zn species. The first group comprises only spectra from bulk LC samples. The bulk PB samples and their grain size fractions, the clay fraction from LC at 168–183 cm depth (LC04) and the river sediment (GE10) are all classified in the second group. The two populations mostly differ in the shape of the third oscillation, with a maximum at ~7.8 $Å^{-1}$ for the first group and a camel-like split structure with a minimum at ~7.6 $Å^{-1}$ for the second group. All spectra from the second group show considerable similarity to the reference spectrum of the trioctahedral phyllosilicate $Si_4(Zn_{2.4}Mg_{0.6})O_{10}(OH)_2.nH_2O$ (ZnKer240), suggesting the predominance of Zn-phyllosilicate in these samples.

Results from the PCA performed on the complete set of twenty-two EXAFS spectra are given in Table 2 and the first five components (C1–C5) are shown in Fig. 3. C1 to C3 oscillate like real EXAFS spectra and have high signal-to-noise ratios, whereas C4 and the following components have little meaningful information. IND reached a minimum for three components, suggesting that only C1 to C3 are linear combinations of real species spectra (Manceau et al., 2002). The NSS_{tot} value decreased by 67 % upon addition of C2 to the one-component C1 fit, 49 % upon addition of C3 to the two-component C1+C2 fit, but only 22 % and 17 % with C4 and C5, respectively. The small decline of NSS_{tot} with C4 and C5 means that these components marginally increased the fit quality, consistent with their low amplitude (Fig. 3). Also, visual examination of all individual fits, and consideration of their NSS values (as low as 0.001 – 0.032 with NSS_{tot} = 0.010), led to the conclusion that all spectral features were well reproduced with the first three components only. Therefore, C1 to C3 were used for target transformation of the reference spectra.

The spectrum of smithsonite ($ZnCO_3$) was best reconstructed (NSS = 0.9 10^{-2}; Fig. 4). Zinc-rich kerolite ($Si_4(Zn_{2.4}Mg_{0.6})O_{10}(OH)_2.nH_2O$, ZnKer240) yielded the best spectral reconstruction (NSS = 1.6 10^{-2}) among the group of references with Zn in an octahedral layer (Zn-containing kerolites, Zn-LDH, Zn-substituted montmorillonite). However, the spectrum of Zn-LDH is close to that of ZnKer240, as a result of the similarity in the local environment of Zn. In both references, Zn is surrounded by approximately the same proportion of Zn and "light" (Al, Mg) atoms in the nearest cationic shell. The difference between the spectra of the two compounds results from the occurrence of tetrahedral sheets in phyllosilicates, for which Zn-rich kerolite (trioctahedral) and Zn-substituted Redhill montmorillonite (dioctahedral) are used as a proxy. The spectrum of ZnKer240 has an oscillation near ~5.2 $Å^{-1}$ caused by the presence of tetrahedral Si, whereas the spectrum of Zn-LDH has only a shoulder at this *k*-value (Schlegel et al., 2001b; Panfili et al., 2005; Schlegel and Manceau, 2006). In the reconstructed spectrum of Zn-LDH (Fig. 4b), an oscillation near ~5.2 $Å^{-1}$, indicative of Zn-phyllosilicate, is clearly present (NSS = 3.5 10^{-2}). Therefore, Zn-LDH was not retained as an acceptable species for LCF. Target testing of pure Zn-kerolite ($Si_4Zn_3O_{10}(OH)_2.nH_2O$, ZnKer300: NSS = 3.2 10^{-2}) was less satisfactory than ZnKer240.

Similarly, kerolites with lower Zn/Mg ratios yielded reconstructions of lower quality relative to ZnKer240 ($Si_4(Zn_{0.03}Mg_{2.97})O_{10}(OH)_2.nH_2O$, ZnKer003: NSS = 23.6 10^{-2}; $Si_4(Zn_{1.35}Mg_{1.65})O_{10}(OH)_2.nH_2O$, ZnKer135: NSS = 4.6 10^{-2}). The reconstruction of Zn-substituted montmorillonite (ZnMontm: NSS = 16.3 10^{-2}) was ten times less good than that of ZnKer240. Thus, target testing indicates that Zn-rich kerolite is the most likely Zn-containing layered mineral. The term "kerolite" is used here as a proxy for the general class of (Zn,Mg) trioctahedral phyllosilicates, including smectites (e.g. stevensite, saponite) because EXAFS is not sensitive to their layer charge.

Target analysis of the complete database showed that Zn is tetrahedral in the third identified species. Zn-sorbed ferrihydrite (ZnFh) gave the best visual reconstruction (Fig. 4a), but with a high NSS value (11.8 10^{-2}) because the signal is weak. Since this species is less certain, the generic term "tetrahedrally coordinated sorbed Zn" (sorbed ^{IV}Zn) will be used in the following to name it, instead of Zn-ferrihydrite. Several other ^{IV}Zn-sorbed species gave similar, or even better, NSS values than ZnFh, but were considered less likely after visual examination of the original and calculated spectra. Of the Zn phosphates tested, Zn-hydroxylapatite reacted at pH 5 (ZnPhos) was reproduced best (NSS = 8.6 10^{-2}), but not accepted because of the phase mismatch of the second oscillation and left side of the third oscillation (Fig. 4b). Also Zn-sorbed montmorillonite (ZnSorbMontm) was rejected due to a phase shift of the second oscillation (NSS = 7.4 10^{-2}). Of the Zn-organic compounds tested, Zn-humic acid and Zn-fulvic acid complexes (ZnHu, ZnFu) yielded the best spectral matches (NSS = 6.2 10^{-2} and NSS = 5.9 10^{-2}, respectively), but the maximum of the first oscillation was right-shifted in the target transforms (k ~ 4.2 Å^{-1} vs. 3.9 Å^{-1}), which is an indication for a difference in Zn coordination (octahedral vs. tetrahedral; Kirpichtchikova et al., 2006). In addition, the second oscillation was not correctly reproduced.

Willemite, hemimorphite and sphalerite, which were detected in some samples by X-ray diffraction (Table 1), did not pass the target test (Fig. 4b; NSS = 29 10^{-2}, 20 10^{-2} and 77 10^{-2}, respectively). In summary, the three species positively identified are smithsonite, Zn-rich kerolite (as a proxy for high-Zn trioctahedral phyllosilicate) and Zn-ferrihydrite (as a proxy for sorbed ^{IV}Zn).

3.3. Quantification of Zn species

The percentage of Zn contained in each species was determined by LCF of the twenty-two EXAFS spectra to the reference spectra of smithsonite, ZnKer240 and Zn-ferrihydrite (Fig. 2; Table 3). The precision in the proportion of Zn contained in each species depends on the amplitude, shape and signal-to-noise ratio of the EXAFS spectra (Sarret et al., 2004). It was estimated here by calculating how much the fit is degraded upon varying the proportions of the reference spectra in the LCF. An increase in NSS of 0.01 had a visible effect on the goodness of fit, as illustrated on Fig. 5a with the bulk spectrum PB30. In this example, the fractional amount of ZnKer240 was varied by 8 % of the total Zn. Fig. 5b shows that this percentage varies with the species, but overall a 10 % precision appears to be a conservative estimate, in agreement with Isaure et al. (2002).

The sum of the fitted fractions varies from 91 to 117 %. Deviations from 100 % of the sum of components reflect the combined effects of the accuracy of the method and the precision on the relative amounts of individual species in a mixture. The accuracy depends on how well the standards represent the unknown sample (i.e. slight differences in local environment of Zn between samples and references), and on errors on the measured (data acquisition) and normalized (data reduction) amplitude of the EXAFS signal (Manceau et al., 2000, 2002). The sums of components for all samples span a range identical (91 %) or slightly in excess (117 %) of the precision (100 % ± 10 %), which engenders confidence in our data analysis. The spectra of the bulk LC samples were simulated with a combination of ~55–60 % smithsonite and ~40–50 % Zn-rich kerolite. The predominance of smithsonite explains the spectral maximum at ~7.8 $Å^{-1}$ noticed previously (Fig. 2). In the bulk PB samples, the fractional amounts of Zn species range from <10 to ~30 % for both smithsonite and sorbed ^{IV}Zn, and from ~60 to ~110 % for Zn-rich kerolite (Fig. 6). Smithsonite occurs mainly in the lower part of the PB profile (depth >107 cm), being absent or in trace amounts (<10 %) in some samples from the upper part. In contrast, sorbed ^{IV}Zn is below detection limit at the bottom of the PB profile, but amounts to 25–30 % of total Zn in the first 81 cm below the surface. Consistent with the small particle size of clays, the proportion of the Zn-rich kerolite pool is systematically higher in the fine (0–2 µm) than in the coarse (0–2 mm) fractions of the LC and PB samples. Hemimorphite was detected by LCF only in the river sediment

(GE10). This species was not identified by target transformation because it is present in only one spectrum and represents only 24 % of the total Zn in the sample.

3.4. pH and Zn concentrations in the 0.01 M $CaCl_2$ extracts

Extractions with 0.01 M $CaCl_2$ were performed on the bulk PB samples. The pH($CaCl_2$) was between 6.1 and 7.4, and Zn concentrations ranged from 0.03 mM to 0.64 mM. Fig. 6c-d shows that the variations in sediment pH follow the variations in the amounts of the Zn-smithsonite pool. Sediments with pH($CaCl_2$) > 7.0 contain ~1500–3000 mg/kg Zn in smithsonite (i.e. ~20–30 % of total Zn), while this pool is below 500 mg/kg (<10 % of total Zn) when pH($CaCl_2$) < 7.0. The correlation between pH and smithsonite abundance is further supported by results from the 0.01 M $CaCl_2$ extractions. When pH($CaCl_2$) > 7.0, the concentration of aqueous Zn corresponds to that in equilibrium with smithsonite (Fig. 7), suggesting that the quantity of Zn dissolved in pore water is controlled by smithsonite solubility. When pH($CaCl_2$) < 7.0, the solutions are undersaturated with respect to smithsonite, but oversaturated or near saturation with respect to Zn-kerolite. Thus, chemical extraction data and solubility calculations are consistent with the mineralogy of the two crystalline Zn phases determined by EXAFS.

4. DISCUSSION

4.1. Zn species and uncertainties in their identification

Three Zn species were used in LCF: smithsonite, Zn-rich kerolite and Zn-ferrihydrite. Smithsonite is primary in origin, whereas Zn-rich kerolite and Zn-ferrihydrite are secondary Zn species. The presence of smithsonite in the two sediment profiles can be explained by the fact that this mineral was mined and smelted upstream in La Calamine. Mineral particles were transported by the river and deposited on the floodplain. Smithsonite was identified previously in dredged sediments by Ndiba et al. (2008) using EXAFS. Sphalerite and franklinite were the main mineral contaminants in other EXAFS studies (Manceau et al., 2000; Isaure et al., 2002, 2005; Roberts et al., 2002; Scheinost et al., 2002; Juillot et al., 2003; Sarret et al., 2004; Nachtegaal et al., 2005). Formation of smithsonite as a secondary species is thermodynamically and kinetically

unlikely (Schindler et al., 1969). The usual Zn carbonate species formed in calcareous settings with high Zn load is hydrozincite ($Zn_5(OH)_6(CO_3)_2$) (Jacquat et al., 2008), by virtue of the higher stability of hydroxylated mineral species at the Earth's surface.

Zinc-rich kerolite-like phyllosilicate is the major form of Zn in most samples. This species has been identified previously in contaminated soils and sediments, and was derived from the in-situ weathering of primary minerals (Manceau et al., 2000; Panfili et al., 2005; Kirpichtchikova et al., 2006; Jacquat et al., 2008). Because of the spectral similarities between ZnKer240, ZnKer300 and Zn-LDH, the mathematical solution obtained by LCF may not be unique. This effect is exemplified with the spectrum of the 0–2 µm fraction of LC04 (Fig. 8). A good fit was obtained with ZnKer240 only (NSS = 1.58 10^{-2}; Table 3). Adding minor Zn-LDH did not improve significantly the fit quality (NSS = 1.54 10^{-2}). However, combining ZnKer300 and Zn-LDH in a 1/1 ratio decreased NSS by more than 50 % (NSS = 0.74 10^{-2}). In the three compounds, octahedral Zn is surrounded by Zn and "light" atoms (Al, Mg) in the second shell, but not in the same proportions. In ZnKer300 ($Si_4Zn_3O_{10}(OH)_2.nH_2O$), Zn has six next-nearest Zn atoms, and in ZnKer240 ($Si_4(Zn_{2.4}Mg_{0.6})O_{10}(OH)_2.nH_2O$), 4.8 Zn and 1.2 Mg on average. In Zn-LDH ($Zn_2Al(OH)_6Cl$), Zn is surrounded either by 4 Zn and 2 Al on average if the cations are distributed at random in the octahedral layer, or by 3 Zn and 3 Al exactly if their distribution is ordered (Bellotto et al., 1996). Thus, if 50 % of Zn is in ZnKer300 and 50 % in Zn-LDH, Zn is surrounded on average by 4.5–5.0 Zn and 1.0–1.5 Al, that is by approximately the same number of "heavy" and "light" (Al, Mg) atoms as in ZnKer240, explaining why EXAFS cannot differentiate between this mixture and pure ZnKer240.

Returning to experimental data, the effect of this indetermination was tested for all twenty-two spectra. In all cases, a better fit was obtained with a mixture of ZnKer300 and Zn-LDH instead of ZnKer240, with 1/3 < ZnKer300 / Zn-LDH < 3/2. However, the hypothesis of two layered Zn species seems unlikely for three reasons. First, Zn-LDH was not acceptably reproduced by target transformation. Second, Zn-Mg kerolites are less soluble than ZnKer300, otherwise Zn would not mix with Mg at the atomic scale to form a solid-solution between the Mg- and Zn-pure end-members (Manceau et al., 2000; Panfili et al., 2005). Third, Zn-Mg kerolites with the same (ZnKer240) and other (ZnKer210, ZnKer135, ZnKer070) average stoichiometries were identified previously in

soils and sediments by micro-EXAFS, resulting in a more definitive identification (Isaure et al., 2002, 2005; Panfili et al., 2005; Kirpichtchikova et al., 2006; Jacquat et al., 2008). Therefore, the predominance of Zn phyllosilicate is most likely, but spectral interference with minor fractions of Zn-LDH can not be ruled out.

Out of the three main Zn species identified in this study, Zn sorbed on ferrihydrite is the least certain. This species has been identified many times in contaminated matrices, and its formation from the weathering of Zn and Fe particles is largely expected in this type of environment. However, the good reconstruction of the ZnFh spectrum by target transformation does not imply that this species exists, because tetrahedral Zn species generally yield similar EXAFS spectra owing to the intensity of the signal from the first oxygen shell (Sarret et al., 2004; Diesing et al., 2008; Jacquat et al., 2008). For instance, Zn-sorbed organic matter is very common in soils and sediments, and can hardly be differentiated from Zn-sorbed ferrihydrite by powder EXAFS.

4.2. Age of the overbank sediments in Plombières

The overbank sediments near Plombières received metals from the different mining and smelting centres along the river, but dominantly from La Calamine (oxidized Zn ores) and Plombières (Pb-Zn sulphides) (Fig. 1). The large-scale activities in Plombières started in 1844. At that time, the La Calamine mine and smelter were already in full operation for several decades (Zn ore production above 4000 ton/year since 1825; Dejonghe et al., 1993). Elevated Pb concentrations (>2000 mg/kg) in the overbank sediments most likely result from the Pb-Zn mining and smelting in Plombières, thus the vertical Pb distribution pattern (Fig. 6b) allows differentiation between sediments deposited before and after 1844. Since the Pb profile shows a marked discontinuity at ~114 cm depth, Zn at deeper depth originates in all likelihood mainly from La Calamine, and Zn above this limit from the two production areas (Fig. 6). The validity of the sediment dating at ~114 cm is verified by the correlation between the upper part of the Pb profile (~25–114 cm) and the yearly production of galena from the Plombières mine over the 1844–1882 period (Dejonghe et al., 1993; Fig. 6b).

Delineation of the sediments deposited before the industrial period (<1806) and after the closure of the major mines (1884) is less evident. The elevated Zn and Pb

concentrations at the bottom of the profile, including the gravel- and clay-rich layer deposited during the Pleistocene (sample PB01; Van de Westeringh, 1980), probably result from the weathering of ore deposits exposed to the surface and from ancient small-scale mining activities. Smelting operations after the closure of the mines, weathering and erosion of waste dumps, and remobilization of upstream contaminated sediments, explain the high Zn and Pb concentrations near the surface. A similar approach to date the overbank sediments of the Geul river using Zn and Pb concentrations was applied by Swennen et al. (1994) and Stam (1999, 2002).

4.3. Downstream change in Zn speciation resulting from La Calamine mining and smelting

The overbank sediments near La Calamine (LC04, LC07, LC09) and the bottom sediments near Plombières (PB02 to PB12) were both contaminated by oxidized Zn minerals. Smithsonite is, however, proportionally much more abundant in the upstream section (LC samples) of the river (~55–60 % of total Zn), where the samples are richer in Zn (29000–69000 mg/kg), than in the downstream section (<30 %), where the samples have less than 12000 mg/kg Zn (Table 3). This positive correlation between smithsonite fraction and total Zn concentration suggests that the ratio of smithsonite to Zn-phyllosilicate in the two sediment columns is controlled by the dissolution rate of the carbonate, since dilution of Zn by uncontaminated sediment would preserve the proportion of smithsonite relative to the total amount of Zn, and the pH does not vary significantly between the two sites (Table 1). Thus, starting from a lower total amount of smithsonite in the downstream sediments, a constant rate of conversion of smithsonite would result in a larger proportion of secondary Zn species at Plombières. Assuming the downstream particles were smaller than at La Calamine, the effect would be enhanced because the dissolution rate of smaller particles is known to be faster.

4.4. Vertical distribution of smithsonite in the Plombières profile

The upper part of the overbank sediments near Plombières (>114 cm; Fig. 6) was contaminated by mining and smelting of Pb-Zn sulphides, in addition to oxidized Zn ores. The amount of Zn as smithsonite decreases from ~1500–3000 mg/kg (~20–30 % of total

Zn) in the deeper sediment (107–183 cm) to <500 mg/kg (<10 % of total Zn) in the upper part (<81 cm). Likely, the upper sediments received less source material from La Calamine because of lower emissions, as attested by the decrease in Zn concentration in the sediment profile near La Calamine from 47000 mg/kg at 100 cm depth to 10000 mg/kg in subsurface (data not shown). Also, the amount of smithsonite at Plombières is correlated with pH($CaCl_2$), as noticed previously (section 3.4). Fig. 6c-d shows that the abrupt diminution of smithsonite at the onset of the Pb-Zn contamination is accompanied by a drop in pH from 7.3–7.4 to 6.4–6.8, which is probably related to the oxidative dissolution of sulphides. Sphalerite and galena were mined in Plombières and other locations in the Geul catchment (Dejonghe, 1993, 1998) and were most probably transported by the river and deposited on the floodplain. The elevated concentrations of Pb and As in the upper PB sediments originate undoubtedly from the sulphide mining acitivities in Plombières, and the presence of sphalerite in the present-day bedload (Table 1) confirms the transport of sulphides by the river. When exposed to oxygen, oxidation and dissolution of sulphides occurs, as shown for example by Isaure et al. (2005), Panfili et al. (2005) and Schuwirth et al. (2007). This chemical reaction results in acidification of the pore water (Smith, 2004), analogous to the processes of acid mine drainage and acid sulphate soils. Here, the decrease in pH is relatively small (at most one unit), because of the large pH buffering capacity of carbonates. Thus, acidic dissolution of smithsonite likely contributed also to the scarcity of this mineral at the top of the sediment column. Similarly, the pre-industrial sediments PB02 and PB03 (193–206 cm) have a low smithsonite content and pH. The lower pH can be explained by the higher organic matter content in the sediments deposited before the large-scale deforestation of the Middle Ages (Van de Westeringh, 1980). In summary, the present speciation of Zn is well explained by the nature of the ore minerals that were mined and smelted in this area at the time of deposition. There is no evidence of an effect of the absolute age of the overbank sediments on the speciation of Zn over the last 200 years.

4.5. Abundance of Zn-phyllosilicate

The overbank sediments of the Geul river have the highest abundance of Zn-rich phyllosilicate identified so far in natural settings. This species was even the only one

detected in some samples (Table 3). Likely, willemite and hemimorphite were a source of dissolved Zn and Si. These Zn-silicates were mined from the ore deposit of La Calamine, together with smithsonite. The carbonate was dominant near the surface, whereas willemite was the major mineral at >80 m depth (reached in 1865; Dejonghe et al., 1993). Hemimorphite was the least abundant of the three ore species. Despite their abundance in the ore deposit, the two primary Zn silicates are today minor Zn species in the overbank sediments of the Geul river. The preservation of smithsonite in proportions up to 60 % of total Zn suggests that willemite and hemimorphite were dissolved to a large extent in the overbank sediments. Thus, their weathering may have promoted the formation of Zn-phyllosilicate. This interpretation cannot be supported by thermodynamic stability calculations because accurate solubility products are lacking for hemimorphite (Brugger et al., 2003; McPhail et al., 2003, 2006) and Zn-rich kerolite (Manceau et al., 2000). Also, the solubility of Zn-LDH, an alternative secondary precipitate, is not well known (Jacquat et al., 2008), further complicating the assessment of the most stable Zn phase at various environmental conditions (pCO_2, Si and Al concentration). However, similar abundance of Zn-phyllosilicate was observed by Manceau et al. (2000) in soils contaminated with willemite and hemimorphite, whereas Zn-phyllosilicates are generally less abundant (< 50 % of total Zn) in soils contaminated by other emission sources (e.g. Panfili et al., 2005; Kirpichtchikova et al., 2006).

The La Calamine ores were cemented with the trioctahedral Zn-phyllosilicate sauconite ($Na_{0.3}Zn_3(Si,Al)_4O_{10}(OH)_2.4(H_2O)$; Coppola et al., 2008). This mineral has a negative layer charge because of substitutions of Al for Si in the tetrahedral sheet, and thus belongs to the smectite group, in contrast to kerolite, which is a disordered hydrated talc with no or little swelling properties (Brindley et al., 1977; Brindley and Brown, 1980). The two phyllosilicates can have the same (Zn,Mg) stoechiometry (Petit et al., 2008), which prevents them from being differentiated by powder EXAFS. Since Zn was contained mainly in smithsonite, willemite and hemimorphite in the La Calamine ores, and only for a minor amount in sauconite (Dejonghe et al., 1993; Coppola et al., 2008), the overbank sediments presumably also contained much more of the primary minerals than sauconite at the time of deposition. The present-day scarcity of willemite and hemimorphite therefore suggests that inherited sauconite represents only a small fraction

of the Zn-kerolite pool, and that the Zn-phyllosilicate is for the most part neoformed. However, since the layer charge of the Zn-phyllosilicate is unknown, the term kerolite-like is more generic, and thus more appropriate.

5. CONCLUSION

Zinc speciation was determined in the overbank sediments of the Geul river, which were contaminated by historical mining and smelting of oxidized Zn ores (smithsonite, willemite, hemimorphite) and Pb-Zn sulphides. EXAFS shows that Zn occurs predominantly in the primary mineral smithsonite, as Zn-containing trioctahedral phyllosilicate, and as surface ^{IV}Zn species sorbed to sediment constituents (e.g. ferrihydrite, organic matter). Smithsonite is persistent in sediments with pH($CaCl_2$) > 7.0, which were contaminated by oxidized Zn ores only. At the onset of additional contamination by Pb-Zn sulphide mining and smelting, (i) the Zn-smithsonite pool decreases from ~1500–3000 mg/kg Zn to <500 mg/kg Zn, (ii) the sorbed ^{IV}Zn pool rises from undetectable to ~1000–3500 mg/kg Zn, and (iii) the pH($CaCl_2$) decreases from 7.3–7.4 to 6.4–6.8. These changes probably result from the oxidation of sulphide minerals, an acid-producing process which promotes the dissolution of smithsonite and other carbonates, and from the adsorption of the dissolved Zn^{2+} as surface complexes. The primary minerals willemite and hemimorphite were not identified by EXAFS in the overbank sediments. The weathering of these two silicates presumably led to the formation of Zn-phyllosilicate. The abundance of Zn-phyllosilicate in the sediments covering 200 years of deposition history attests to the stability of this Zn phase, as long as the current environmental conditions (including the near neutral pH) are preserved. Changes in the soil chemistry, such as acidification, could cause the release of Zn^{2+} by dissolution of the Zn-phyllosilicate phase. However, this process is unlikely to occur as long as there are carbonates to buffer the pH. This study shows how information on contamination history and EXAFS can be combined to understand the weathering process of primary Zn minerals in overbank sediments.

Acknowledgments

The authors thank Drs. F. Panfili, A. Scheinost, A. Voegelin and their co-workers for providing EXAFS spectra of Zn references. The staff of beamline BM26A (DUBBLE) and Dr. G. Cornelis are acknowledged for the help with EXAFS data acquisition. We thank the NWO (Netherlands Organisation for Scientific Research) and FWO-Vlaanderen (Fund for Scientific Research-Flanders) for the provision of beamtime at DUBBLE/ESRF and for the financial support. A. Van Damme and F. Degryse acknowledge the FWO-Vlaanderen for a position as research assistant and postdoctoral researcher, respectively. This manuscript benefitted from the constructive remarks of three anonymous reviewers.

REFERENCES

Allison J. D., Brown D. S. and Novo-Gradac K. J. (1991) *MINTEQA2/PRODEFA2, A Geochemical Assessment Model for Environmental Systems.* U.S. Environmental Protection Agency.

Bellotto M., Rebours B., Clause O., Lynch J., Bazin D. and Elkaïm E. (1996) A reexamination of hydrotalcite crystal chemistry. *J. Phys. Chem.* **100**: 8527-8534.

Brindley G. W. and Brown G. (1980) *Crystal structures of clay minerals and their X-ray identification*. Mineralogical Society, London.

Brindley G. W., Bish D. L. and Wan H.-M. (1977) The nature of kerolite, its relation to talc and stevensite. *Mineral. Mag.* **41:** 443-452.

Brugger J., McPhail D. C., Wallace M. and Waters J. (2003) Formation of Willemite in Hydrothermal Environments. *Econ. Geol.* **98**: 819-835.

Coppola V., Boni M., Gilg H. A., Balassone G. and Dejonghe L. (2008) The "calamine" nonsulfide Zn–Pb deposits of Belgium: Petrographical, mineralogical and geochemical characterization. *Ore Geol. Rev.* **33***,* 187-210.

D'Amore J. J., Al-Abed S. R., Scheckel K. G. and Ryan J. A. (2005) Methods for speciation of metals in soils: A review. *J. Environ. Qual.* **34**: 1707-1745.

Degryse F., Broos K., Smolders E. and Merckx R. (2003) Soil solution concentration of Cd and Zn can be predicted with a $CaCl_2$ soil extract. *Eur. J. Soil Sci.* **54**: 149-158.

Dejonghe L. (1998) Zinc-lead deposits of Belgium. *Ore Geol. Rev.* **12**, 329-354.

Dejonghe L., Ladeuze F. and Jans, D. (1993) Atlas des gisements plombo-zincifères du Synclinorium de Verviers (Est de la Belgique). *Mémoires pour servir à l'Explication des Cartes Géologiques et Minières de la Belgique* **33**, 1-483.

Diesing W. E., Sinaj S., Sarret G., Manceau A., Flura T., Demaria P., Siegenthaler A., Sappin-Didier V. and Frossard E. (2008) Zinc speciation and isotopic exchangeability in soils polluted with heavy metals. *Eur. J. Soil Sci.* **59**, 716-729.

Horckmans L., Swennen R. and Deckers J. (2007) Retention and release of Zn and Cd in spodic horizons as determined by pH_{stat} analysis and single extractions. *Sci. Total Environ.* **376**: 86-99.

Houba V. J. G., Lexmond Th. M., Novozamsky I. and van der Lee J. J. (1996) State of the art and future developments in soil analysis for bioavailability assessment. *Sci. Total Environ.*, **178**: 21-28.

Isaure M.-P., Laboudigue A., Manceau A., Sarret G., Tiffrau C., Trocellier P., Lamble G. M., Hazemann J. L. and Chateigner D. (2002) Quantitative Zn speciation in a contaminated dredged sediment by μ-PIXE, μ-SXRF, EXAFS spectroscopy and principal component analysis. *Geochim. Cosmochim. Acta* **66**, 1549-1567.

Isaure M.-P., Manceau A., Geoffroy N., Laboudigue A., Tamura N. and Marcus M. A. (2005) Zinc mobility and speciation in soil covered by contaminated dredged sediment using micrometer-scale and bulk-averaging X-ray fluorescence, absorption and diffraction techniques. *Geochim. Cosmochim. Acta* **69**, 1173-1198.

Jacquat O., Voegelin A., Villard A., Marcus M. A. and Kretzschmar R. (2008) Formation of Zn-rich phyllosilicate, Zn-layered double hydroxide and hydrozincite in contaminated calcareous soils. *Geochim. Cosmochim. Acta* **72**, 5037-5054.

Jacquat O., Voegelin A., Kretzschmar R. (2009) Soil properties controlling Zn speciation and fractionation in contaminated soils. *Geochim. Cosmochim. Acta* **73**, 5256-5272.

Juillot F., Morin G., Ildefonse P., Trainor T. P., Benedetti M., Galoisy L., Calas G. and Brown G. E. (2003) Occurrence of Zn/Al hydrotalcite in smelter-impacted soils from northern France: evidence from EXAFS spectroscopy and chemical extractions. *Am. Mineral.* **88**, 509-526.

Kirpichtchikova T. A., Manceau A., Spadini L., Panfili F., Marcus M. A. and Jacquet T. (2006) Speciation and solubility of heavy metals in contaminated soil using X-ray microfluorescence, EXAFS spectroscopy, chemical extraction, and thermodynamic modeling. *Geochim. Cosmochim. Acta* **70**, 2163-2190.

Konert M. and Vandenberghe J. (1997) Comparison of laser grain size analysis with pipette and sieve analysis: a solution for the underestimation of the clay fraction. *Sedimentology* **44**, 523-535.

Kucha H., Martens A., Ottenburgs R., De Vos W. and Viaene W. (1996) Primary minerals of Zn-Pb mining and metallurgical dumps and their environmental behavior at Plombières, Belgium. *Environ. Geol.* **27**: 1-15.

Leenaers H. (1989) The dispersal of metal mining wastes in the catchment of the river Geul (Belgium- the Netherlands). *Netherlands Geographical Studies* **102**: 1-200.

Malinowski E. R. (1977) Determination of the number of factors and the experimental error in a data matrix. *Anal. Chem.* **49**: 612-617.

Malinowski E.R. (1978) Theory of error for target factor analysis with applications to mass spectrometry and nuclear magnetic resonance spectrometry. *Anal. Chim. Acta* **103**, 339-354.

Manceau A., Bonnin D., Stone W. E. E. and Sanz J. (1990) Distribution of Fe in the octahedral sheet of trioctahedral micas by polarized EXAFS. *Phys. Chem. Miner.* **17**: 363-370.

Manceau A., Boisset M. C., Sarret G., Hazemann J. L., Mench M., Cambier Ph. and Prost R. (1996) Direct determination of lead speciation in contaminated soils by EXAFS spectroscopy. *Environ. Sci. Technol.*, **30**: 1540-1552.

Manceau A., Lanson B., Schlegel M. L., Harge J. C., Musso M., Eybert-Berard L., Hazemann J. L., Chateigner D. and Lamble G. M. (2000) Quantitative Zn speciation in smelter-contaminated soils by EXAFS spectroscopy. *Am. J. Sci.* **300**, 289-343.

Manceau A., Marcus M. A. and Tamura N. (2002) Quantitative speciation of heavy metals in soils and sediments by synchrotron X-ray techniques. In *Applications of Synchrotron Radiation in Low-Temperature Geochemistry and Environmental Science* (eds. P. Fenter, S. Sutton, M. Rivers and N. C. Sturchio). Rev. Mineral. Geochem. 49, 341-428.

Manceau A., Tommaseo C., Rihs S., Geoffroy N., Chateigner D., Schlegel M. L., Tisserand D., Marcus M. A., Tamura N. and Zueng-Sang C. (2005) Natural speciation of Mn, Ni, and Zn at the micrometer scale in a clayey paddy soil using X-ray fluorescence, absorption, and diffraction. *Geochim. Cosmochim. Acta* **60**, 4007-4034.

Manceau A. and Matynia A. (2010) The nature of Cu bonding to natural organic matter. *Geochim. Cosmochim. Acta*, in press.

Marcus M. A., MacDowell A. A., Celestre R., Manceau A., Miller T., Padmore H. A. and Sublett R. E. (2004) Beamline 10.3.2 at ALS: a hard X-ray microprobe for environmental and materials sciences. *J. Synchrotron Radiat.* **11**: 239-247

McPhail D. C., Summerhayes E., Welch S. and Brugger J. (2003) The geochemistry and mobility of zinc in the regolith. In *Advances in Regolith* (ed. I.C. Roach). CRC LEME, Bentley. pp. 287-291.

McPhail D. C., Summerhayes E., Jayaratne V. and Christy A. (2006) Hemimorphite solubility and stability of low-T zinc minerals. *Geochim. Cosmochim. Acta* **70**: A414.

Miller J. R. and Orbock Miller S. M. (2007) *Contaminated Rivers: A Geomorphological-Geochemical Approach to Site Assessment and Remediation*. Springer, Dordrecht.

Nachtegaal M., Marcus M. A., Sonke J. E., Vangronsveld J., Livi K. J. T., Van der Lelie D. and Sparks D. L. (2005) Effects of in situ remediation on the speciation and bioavailability of zinc in a smelter contaminated soil. *Geochim. Cosmochim. Acta* **69**, 4649-4664.

Ndiba P., Axe L. and Boonfueng T. (2008) Heavy metal immobilization through phosphate and thermal treatment of dredged sediments. *Environ. Sci. Technol.* **42**: 920-926.

Nelson D. W. and Sommers L. E. (1982) Total carbon, organic carbon, and organic matter. In *Methods of soil analysis, Part 2: chemical and microbiological properties* (eds. A. L. Page, R. H. Miller and D. R. Keeney). American Society of Agronomy, Madison. pp. 539-579.

Newville M. (2001) IFEFFIT: interactive XAFS analysis and FEFF fitting. *J. Synchrotron Radiat.* **8**, 322-324.

Nikitenko S., Beale A. M., van der Eerden A. M. J., Jacques S. D. M., Leynaud O., O'Brien M. G., Detollenaere D., Kaptein R., Weckhuysen B. M. and Bras W. (2008) Implementation of a combined SAXS/WAXS/QuEXAFS set-up for time-resolved in situ experiments. *J. Synchrotron Radiat.* **15**: 632-640.

Ottesen R. T., Bogen J., Bolviken B. and Volden T. (1989) Overbank sediment: a representative sample medium for regional geochemical mapping. *J. Geochem. Explor.* **32**, 257-277.

Panfili F. R., Manceau A., Sarret G., Spadini L., Kirpichtchikova T., Bert V., Laboudigue A., Marcus M. A., Ahamdach N. and Libert M. F. (2005) The effect of phytostabilization on Zn speciation in a dredged contaminated sediment using scanning electron microscopy, X-ray fluorescence, EXAFS spectroscopy, and principal components analysis. *Geochim. Cosmochim. Acta* **69**, 2265-2284.

Petit S., Righi D. and Decarreau A. (2008) Transformation of synthetic Zn-stevensite to Zn-talc induced by the Hofmann-Klemen effect. *Clays Clay Miner.* **56**: 645-654.

Quevauviller, Ph. (1998) Operationally defined extraction procedures for soil and sediment analysis I. Standardization. *Trends Anal. Chem.* **17**, 289-298.

Ravel B. and Newville M. (2005) Athena, Artemis, Hephaestus: data analysis for X-ray absorption spectroscopy using IFEFFIT. *J. Synchrotron Radiat.* **12**, 537-541.

Ressler T., Wong J., Roos J. and Smith I. L. (2000) Quantitative speciation of Mn-bearing particulates emitted from autos burning (methylcyclopentadienyl)manganese tricarbonyl-added gasolines using XANES spectroscopy. *Environ. Sci. Technol.*, **34**: 950-958.

Roberts D. R., Scheinost A. C. and Sparks D. L. (2002) Zinc speciation in a smelter-contaminated soil profile using bulk and microspectroscopic techniques. *Environ. Sci. Technol.* **36**, 1742-1750.

Sarret G., Saumitou-Laprade P., Bert V., Proux O., Hazemann J. L., Traverse A., Marcus M. A. and Manceau A. (2002) Forms of Zn accumulated in the hyperaccumulator *Arabidopsis halleri*. *Plant Physiol.* **130**, 1815-1826.

Sarret G., Balesdent J., Bouziri L., Garnier J. M., Marcus M. A., Geoffroy N., Panfili F. and Manceau A. (2004) Zn speciation in the organic horizon of a contaminated soil by micro-X-ray fluorescence, micro- and powder-EXAFS spectroscopy, and isotopic dilution. *Environ. Sci. Technol.* **38**, 2792-2801.

Scheinost A. C., Kretzschmar R., Pfister S. and Roberts D. R. (2002) Combining selective sequential extractions, X-ray absorption spectroscopy, and principal component analysis for quantitative zinc speciation in soil. *Environ. Sci. Technol.* **36**, 5021-5028.

Schindler P., Reinert M. and Gamsjäger H. (1969) Löslichkeitskonstanten und freie Bildungsenthlapien von $ZnCO_3$ und $Zn_5(OH)_6(CO_3)_2$ bei 25 °C. *Helv. Chim. Acta* **52**, 2327-2332.

Schlegel M. L. and Manceau A. (2006) Evidence for the nucleation and epitaxial growth of Zn phyllosilicate on montmorillonite. *Geochim. Cosmochim. Acta* **70**, 901-917.

Schlegel M. L., Manceau A., Charlet L. and Hazemann J. L. (2001a) Adsorption mechanisms of Zn on hectorite as a function of time, pH, and ionic strength. *Am. J. Sci.* **301**, 798-830.

Schlegel M. L., Manceau A., Charlet L., Chateigner D. and Hazemann J. L. (2001b) Sorption of metal ions on clay minerals. III. Nucleation and epitaxial growth of Zn phyllosilicate on the edges of hectorite. *Geochim. Cosmochim. Acta* **65**, 4155-4170.

Schuwirth N., Voegelin A., Kretzschmar R. and Hofmann T. (2007) Vertical distribution and speciation of trace metals in weathering flotation residues of a zinc/lead sulfide mine. *J. Environ. Qual.* **36**, 61-69.

Smith J. (2004) Chemical changes during oxidation of iron monosulfide-rich sediments. *Aust. J. Soil Res.* **42**: 659-666.

Stam M. H. (1999) The dating of fluvial deposits with heavy metals, Pb-210 Cs-137 in the Geul catchment (The Netherlands). *Phys. Chem. Earth. PT B* **24**: 155-160.

Stam M. H. (2002) Effects of land-use and precipitation changes on floodplain sedimentation in the nineteenth and twentieth centuries (Geul River, The Netherlands). *Spec. Publ. IAS* **32**: 251-267.

Swennen R. and Viaene W. (1990) Lithogeochemical patterns around Pb-Zn mineralizations in Dinantian carbonate rocks of (eastern) Belgium. *Mineral. Deposita* **25**, 251-261.

Swennen R., Van Keer I. and De Vos W. (1994) Heavy metal contamination in overbank sediments of the Geul river (East Belgium): Its relation to former Pb-Zn mining activities. *Environ. Geol.* **24**, 12-21.

Van de Westeringh W. (1980) Soils and their geology in the Geul Valley. In *Soil conditions, soil carbonates and former vegetation in the Geul valley from Gulpen*

to Meerssen (South Limburg, The Netherlands) (ed. W. Van de Westeringh). Mededelingen Landbouwhogeschool Wageningen 80, 1-25.

Van Herreweghe S., Swennen R., Cappuyns V. and Vandecasteele C. (2002) Chemical associations of heavy metals and metalloids in contaminated soils near former ore treatment plants: a differentiated approach with emphasis on pHstat-leaching. *J. Geochem. Explor.* **76**: 113-138.

Voegelin A., Pfister S., Scheinost A. C., Marcus M. A. and Kretzschmar R. (2005) Changes in zinc speciation in field soil after contamination with zinc oxide. *Environ. Sci. Technol.* **39**, 6616-6623.

Wasserman S. R., Allen P. G., Shuh D. K., Bucher J. J. and Edelstein N. M. (1999) EXAFS and principal component analysis: a new shell game. *J. Synchrotron Radiat.* **6**: 284-286.

Table 1: Physico-chemical characteristics of sediment samples.

Sampling site	La Calamine (LC)	Plombières (PB)					Border B-Nl
Sediment type	Overbank sediment	Overbank sediment					River sediment
Depth interval	0 – 228 cm	0 – 59 cm[a]	59 – 114 cm[a]	114 – 183 cm[a]	183 – 206 cm[a]	206 – 225 cm[a]	-
Samples analysed using EXAFS	LC04 LC07 LC09	PB21 PB30 PB32	PB12 PB17 PB20	PB05 PB08 PB11	PB02 PB03	PB01	GE10
Description	Loam, (sandy loam)[b] Brown, (brownish black)[b]	Sandy loam Dark brown	Loam Brown	Loam Brown	Loam Brown	Sandy clay Gray	Coarse sand Brownish black
Zn (mg/kg)	10000 – 69000	4000 – 12000	5200 – 12000	7800 – 12000	5200 – 6600	7600	3200
Pb (mg/kg)	410 – 2200	2100 – 5400	530 – 3000	330 – 430	400 – 1200	1800	600
Cd (mg/kg)	6 – 18	9 – 29	7 – 23	4 – 12	4 – 5	6	5
As (mg/kg)	11 – 38	32 – 89	12 – 18	12 – 13	13 – 19	5	25
Cu (mg/kg)	15 – 24	32 – 73	14 – 28	12 – 13	12 – 18	14	19
Mn (mg/kg)	440 – 2300	350 – 570	400 – 450	380 – 510	210 – 640	66	340
Fe (%)	1.7 – 3.5	1.7 – 2.9	1.6 – 1.9	1.7 – 1.9	1.9 – 2.7	1.1	1.5
Ca (%)	0.67 – 1.1	0.31 – 0.50	0.26 – 0.55	0.25 – 0.35	0.23 – 0.32	0.32	0.70
Mg (%)	0.29 – 0.56	0.10 – 0.13	0.08 – 0.14	0.08 – 0.12	0.08 – 0.12	0.11	0.20
K (%)	0.85 – 1.3	0.84 – 1.2	1.1 – 1.3	1.0 – 1.4	1.1 – 1.3	1.2	0.72
Al (%)	3.7 – 4.7	1.1 – 3.9	2.1 – 2.6	2.2 – 2.8	1.9 – 3.2	3.1	nd
S (%)	<0.1	<0.1 – 0.2	<0.1	<0.1	<0.1	<0.1	nd
Org C (%)	0.6 – 4.4	2.0 – 3.8	1.1 – 2.2	0.9 – 1.1	0.9 – 2.7	0.4	1.3
pH(water)	7.2 – 7.8	6.7 – 7.6	6.9 – 7.6	7.7 – 8.0	7.2 – 7.4	7.6	7.7
pH($CaCl_2$)	nd	6.1 – 6.8	6.4 – 7.1	7.2 – 7.4	6.7 – 6.8	7.4	nd
Clay (vol%)[c]	nd	20 – 25	18 – 22	19 – 21	18 – 22	42	16
Silt (vol%)	nd	30 – 40	33 – 38	37 – 40	29 – 31	32	17
Sand (vol%)	nd	38 – 48	40 – 47	38 – 43	49 – 52	26	67
Zn-minerals[d]	smithsonite hemimorphite	smithsonite hemimorphite willemite	nd	smithsonite	nd	nd	smithsonite hemimorphite willemite sphalerite

nd: not determined. [a] The PB samples were grouped in depth intervals using boundaries of sedimentary units and noteworthy differences in Zn or Pb concentration (Fig. 6a). [b] Descriptions between brackets only apply to the upper 20 cm interval. [c] 0–8 µm fraction, taking into account the underestimation of the clay content by laser diffractometry (Konert and Vandenberghe, 1997). [d] Identified using XRD on bulk samples and/or concentrates, separated by sieving (125–250 µm), density (d > 2.9 g/mL) and magnetic fractionation.

Table 2: Results of the principal component analysis of the twenty-two EXAFS spectra.

C[a]	Eigenvalue	IND[b]	NSS_{tot}[c] ($\times 10^2$)
1	169	0.0209	5.87
2	34.6	0.0135	1.92
3	16.9	0.0109	0.971
4	8.09	0.0110	0.755
5	6.18	0.0116	0.628
6	5.47	0.0124	0.529
7	5.18	0.0133	0.441
8	4.58	0.0145	0.372

[a] Component. [b] Indicator value (Malinowski, 1977, 1978).

[c] $NSS_{tot} = \Sigma_{spectra}\Sigma_i[k^3\chi(k_i)_{exp} - k^3\chi(k_i)_{reconstr}]^2 / \Sigma_{spectra}\Sigma_i[k^3\chi(k_i)_{exp}]^2$

Table 3: Proportions of Zn species determined by linear combination fitting.

Sample	P.s. fr.[a] (mm)	Depth (cm)	Total Zn (mg/kg)	Sm[b] (%)	ZnKer240[c] (%)	^{IV}Zn[d] (%)	Sum (%)	NSS[e] ($\times 10^2$)
PB01	0–2	206–225	7600	19	72	10	101	3.38
PB02	0–2	203–206	6600	-	107	-	107	3.32
PB03	0–2	193–203	5700	-	108	-	108	3.02
PB05	0–2	173–183	7800	22	83	-	105	2.76
PB08	0–2	147–155	10300	22	82	-	104	1.61
	0–0.002	147–155	nd	-	113	-	113	1.87
PB11	0–2	114–125	9800	29	66	8	103	1.95
PB12	0–2	107–114	8300	28	69	13	110	4.35
PB17	0–2	75–81	5200	7	73	26	106	3.09
PB20	0–2	59–64	12000	-	71	24	95	2.65
PB21	0–2	55–59	12200	-	63	28	91	3.12
	1–2	55–59	16400	6	72	27	105	1.34
	0.125–0.250	55–59	11200	-	66	25	91	3.26
	0–0.002	55–59	nd	-	100	11	111	1.39
PB30	0–2	13–19	7100	7	56	30	93	3.73
	0–0.002	13–19	nd	-	86	20	106	1.53
PB32	0–2	0–7	4000	-	67	30	97	3.18
LC04	0–2	168–183	69000	55	47	-	102	0.816
	0–0.002	168–183	nd	-	117	-	117	1.58
LC07	0–2	123–138	29000	58	50	-	108	0.881
LC09	0–2	93–108	47000	60	38	12	110	0.899
GE10	0–2	-	3200	21	63	24[f]	108	4.20

nd: not determined. [a] Particle size fraction. [b] Smithsonite ($ZnCO_3$). [c] Zn-rich kerolite ($Si_4(Zn_{2.4}Mg_{0.6})O_{10}(OH)_2.nH_2O$). [d] Tetrahedrally coordinated sorbed Zn, with ZnFh as proxy. [e] $NSS = \Sigma_i[k^3\chi(k_i)_{exp} - k^3\chi(k_i)_{reconstr}]^2 / \Sigma_i[k^3\chi(k_i)_{exp}]^2$. [f] Refers to hemimorphite, not ^{IV}Zn. Smithsonite and sorbed ^{IV}Zn fractions between 5 and 10 % may not be significant.

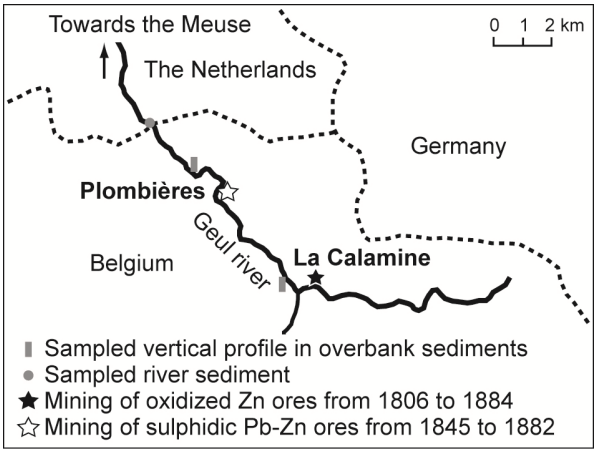

Fig. 1. Geographical setting of the Geul river, sampling sites and major mines. Mining already took place in the Middle Ages, and reached its apogee during the 19th century. Smelters were located nearby the mines.

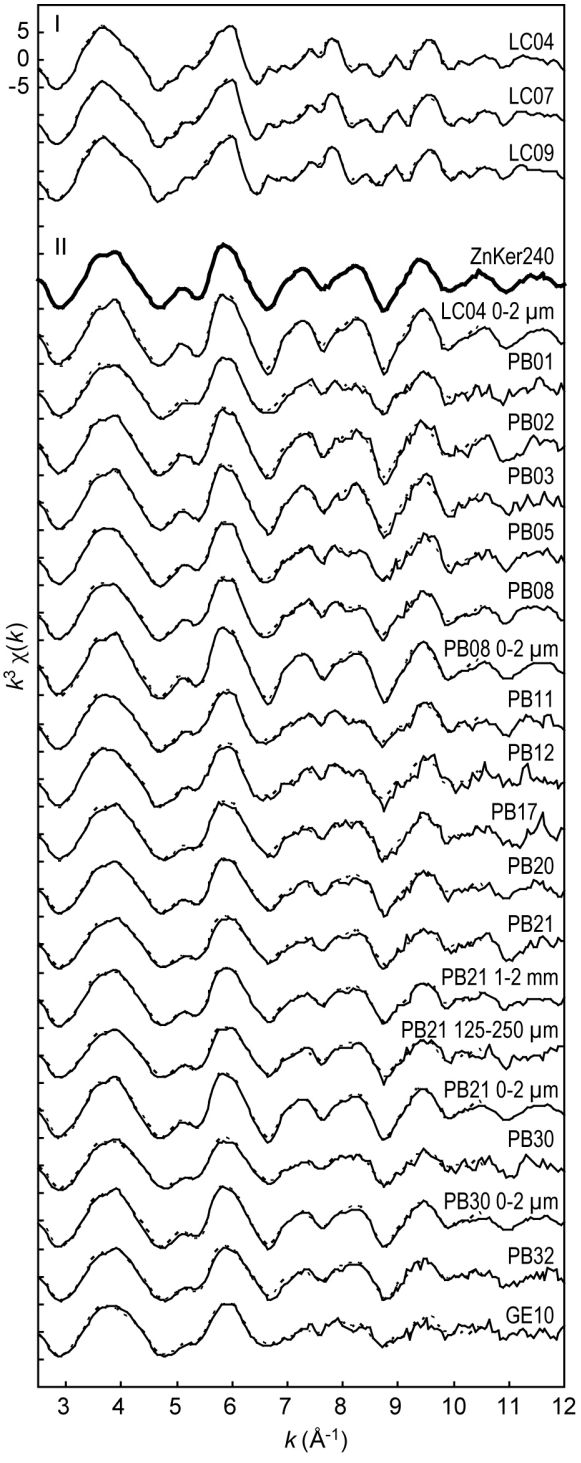
I
II
LC04
LC07
LC09
ZnKer240
LC04 0-2 µm
PB01
PB02
PB03
PB05
PB08
PB08 0-2 µm
PB11
PB12
PB17
PB20
PB21
PB21 1-2 mm
PB21 125-250 µm
PB21 0-2 µm
PB30
PB30 0-2 µm
PB32
GE10
5
0
-5
3
4
5
6
7
8
9
10
11
12
k (Å-1)
k3 χ(k)

Fig. 2.

Fig. 2. Powder Zn K-edge k^3-weighted EXAFS spectra (full lines) and LCF simulations (dashed lines). The proportions of Zn species are reported in Table 3. The particle size fraction is 0–2 mm, unless stated otherwise. Spectra are classified into two groups according to their shape in the *k*-interval ~7–8.5 $Å^{-1}$. The spectra of the second group show similarities with Zn-containing kerolite ($Si_4(Zn_{2.4}Mg_{0.6})O_{10}(OH)_2.nH_2O$, ZnKer240).

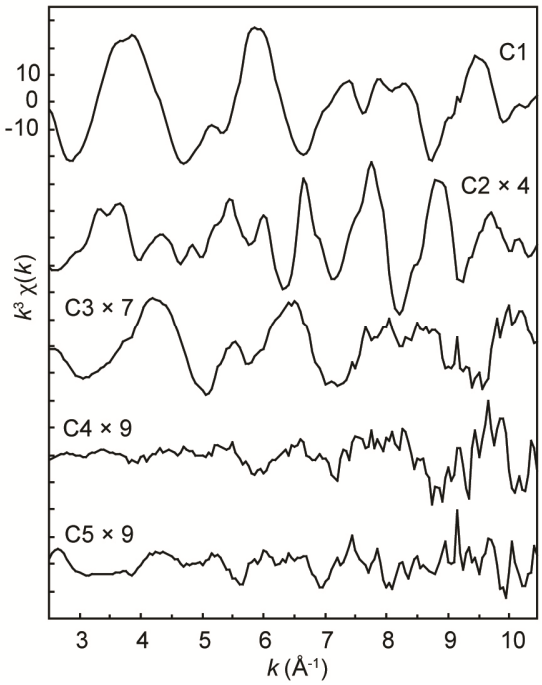

Fig. 3. First five principal components (C1–C5) weighted by eigenvalues for the twenty-two $k^3\chi(k)$ spectra shown in Fig. 2. For clarity, the amplitudes of C2, C3, C4 and C5 were multiplied by 4, 7, 9 and 9, respectively.

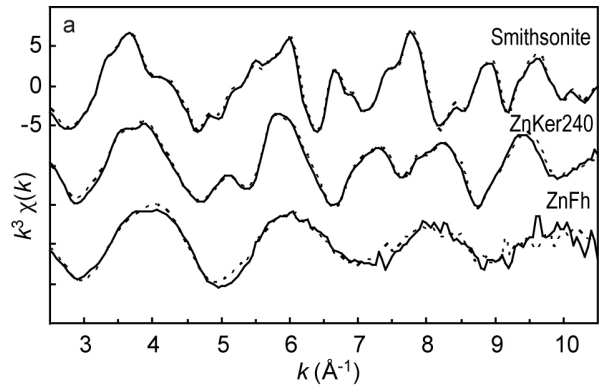
a
Smithsonite
ZnKer240
ZnFh
5
0
-5
$k^3\chi(k)$
3
4
5
6
7
8
9
10
k (Å^{-1})

Fig. 4a.

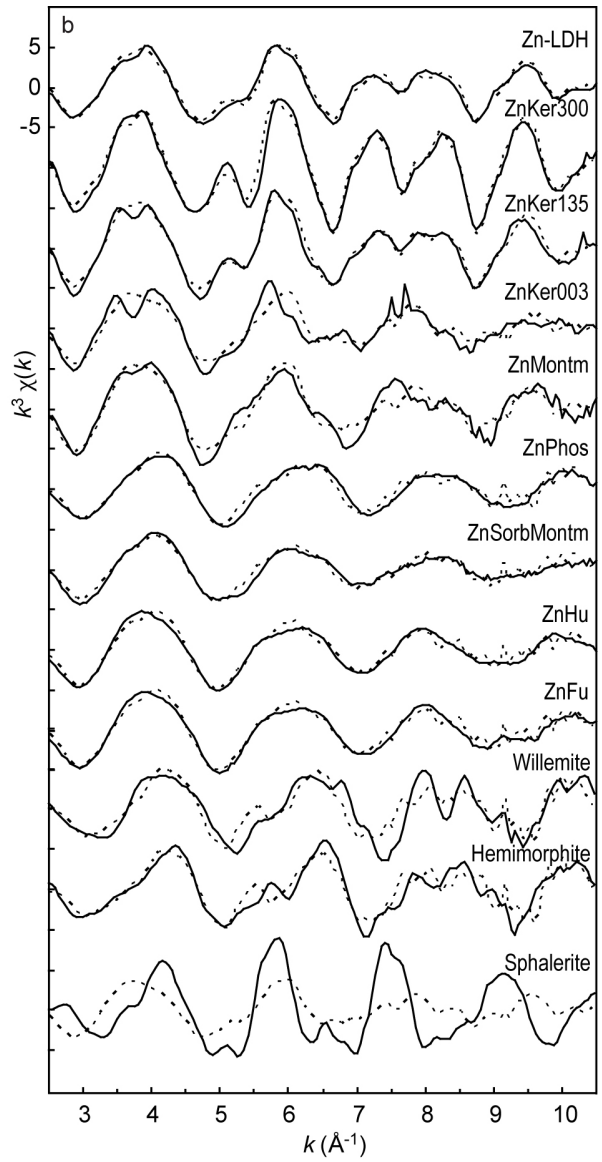
b
Zn-LDH
ZnKer300
ZnKer135
ZnKer003
ZnMontm
ZnPhos
ZnSorbMontm
ZnHu
ZnFu
Willemite
Hemimorphite
Sphalerite
5
0
-5
$k^3\chi(k)$
3
4
5
6
7
8
9
10
k (Å^{-1})

Fig. 4b.

Fig. 4. Zn K-edge EXAFS spectra (full lines) and target transformations (dashed lines) of Zn reference compounds. (a) Successful target transformations: smithsonite ($ZnCO_3$), Zn-rich kerolite ($Si_4(Zn_{2.4}Mg_{0.6})O_{10}(OH)_2.nH_2O$, ZnKer240), Zn-sorbed ferrihydrite (ZnFh); (b) Less or unsuccessful target transformations (selection): Zn layered double hydroxide ($Zn_2Al(OH)_6Cl$, Zn-LDH), low Zn-containing kerolite ($Si_4(Zn_{0.03}Mg_{2.97})O_{10}(OH)_2.nH_2O$, ZnKer003), medium Zn-containing kerolite ($Si_4(Zn_{1.35}Mg_{1.65})O_{10}(OH)_2.nH_2O$, ZnKer135), pure Zn-kerolite ($Si_4Zn_3O_{10}(OH)_2.nH_2O$, ZnKer300), Zn-substituted montmorillonite (ZnMontm), Zn-reacted hydroxylapatite ($Ca_{10}(PO_4)_6(OH)_2$) (ZnPhos), Zn-sorbed montmorillonite (ZnSorbMontm), Zn-humic acid (ZnHu), Zn-fulvic acid (ZnFu), willemite (Zn_2SiO_4), hemimorphite ($Zn_4Si_2O_7(OH)_2.H_2O$) and sphalerite (ZnS).

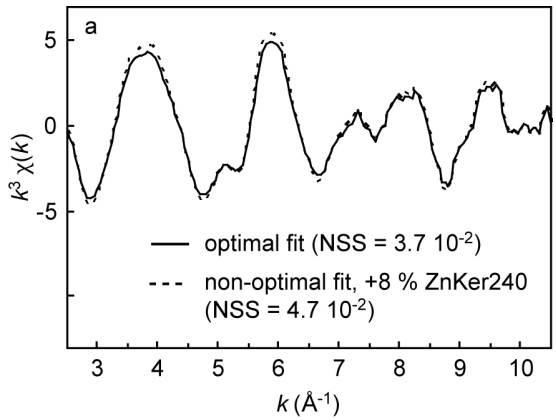

Fig. 5a.

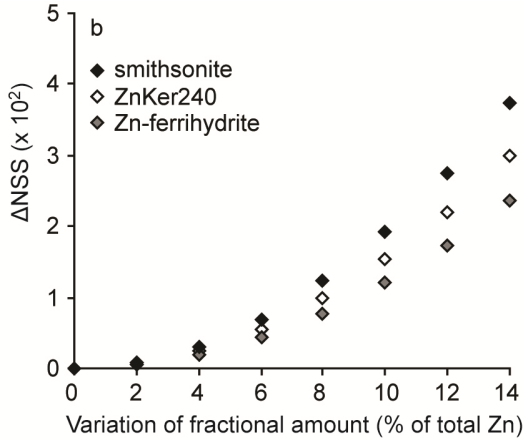

Fig. 5b.

Fig. 5. Evaluation of the precision on the proportion of smithsonite, ZnKer240 and ZnFh determined by LCF, illustrated with the bulk spectrum PB30. The NSS value was calculated for successive linear combinations, each deviating from the optimal fit in the proportion of one species at a time. (a) An increase in the NSS of 0.01, obtained here by increasing the optimal proportion of ZnKer240 by 8 % of total Zn, clearly degraded the fit. Therefore, the value of 0.01 was retained to estimate the precision on the proportion of each species. (b) The deviation of NSS (ΔNSS; Y-axis) from its optimal value (Table 3) upon variation of the fractional amount of one species (X-axis).

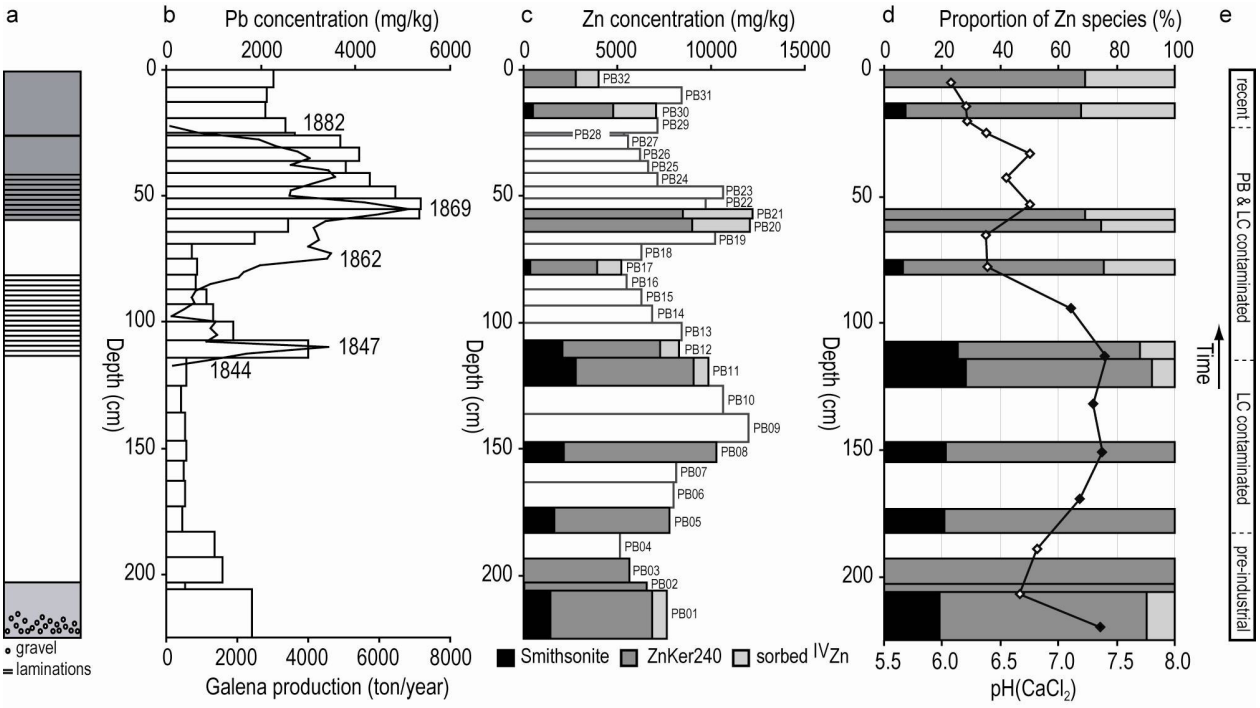

Fig. 6. Vertical profile in overbank sediments near Plombières. (a) Schematic overview (sediment colors are given in Table 1). (b) Concentrations of Pb (bars), and galena production of the Plombières mine (full line; Dejonghe et al., 1993). The two patterns could be matched by assuming a constant sedimentation rate of 2.5 cm/year, allowing approximative dating of the sediment column. (c) Concentrations of Zn (bars) and results from the LCF analysis in absolute values (normalized fraction multiplied by total Zn concentration). (d) Results from the LCF analysis as percentage of total Zn (bars; the sum of Zn species was normalized to 100 % to facilitate comparison between samples), and pH($CaCl_2$) (open and closed symbols as in Fig. 7). (e) Estimated relationship between sediment depth and contamination history: 'pre-industrial' – deposition before the start of industrial operations; 'LC contaminated' – contamination mainly with oxidized Zn minerals from the La Calamine mine; 'PB & LC contaminated' – co-contamination with Pb-Zn sulphides from Plombières in addition to oxidized Zn ores; 'recent'- deposition after the cessation of most industrial activities.

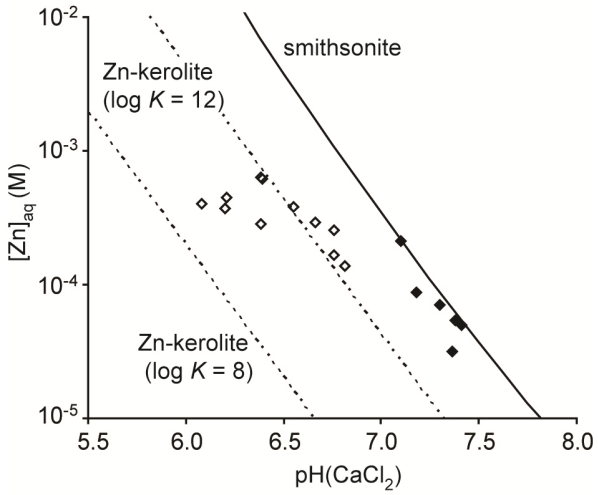

Fig. 7. Zinc concentrations in 10^{-2} M $CaCl_2$ extracts of the PB samples (symbols) and predicted values at equilibrium with smithsonite (log K = 10.9) and with Zn-kerolite (log K = 8 and 12) (lines) at CO_2 partial pressure of 10^{-3} atm, and Si and $CaCl_2$ concentrations of 10^{-4} M and 10^{-2} M, respectively. At pH($CaCl_2$) > 7.0 (closed symbols), the aqueous Zn concentration seems to be controlled by smithsonite dissolution, whereas at pH($CaCl_2$) < 7.0 (open symbols), aqueous Zn is potentially controlled by Zn-kerolite or sorbed Zn. Solubility data are consistent with EXAFS results, because smithsonite amounts to >20 % of Zn in samples with pH > 7.0, and <10 % in samples with pH < 7.0 (Fig. 6d).

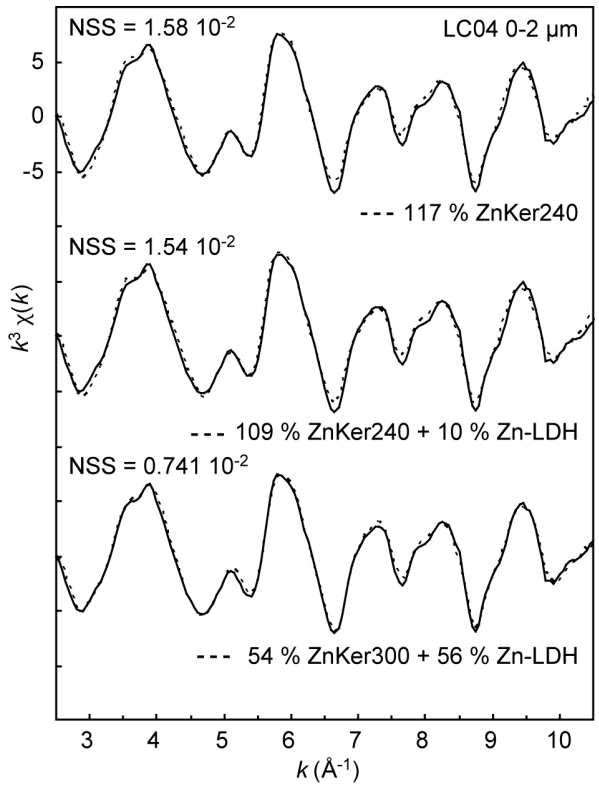

Fig. 8. Zn K-edge EXAFS spectrum of the 0–2 µm fraction for LC04 (full lines) with fits using different combinations of ZnKer240, ZnKer300 and Zn-LDH (dashed lines). Although the best fit was obtained with a one-to-one mixture of ZnKer300 and Zn-LDH, differences are minor and this mathematical solution probably is mineralogically incorrect (see main text for discussion).